# Low-Frequency Controls on the Thresholds of Sea Surface Temperature over the Western Tropical Pacific

NIHAT CUBUKCU AND T. N. KRISHNAMURTI

*Department of Meteorology, The Florida State University, Tallahassee, Florida*

(Manuscript received 11 May 2001, in final form 14 January 2002)

ABSTRACT

In this study, the Florida State University Coupled Global Spectral Model (FSUCGSM) is utilized to examine the possible regulation of the warm pool SST and its contributors. The model is run for 1 yr to obtain the residue-free time evolution of the warm pool SST. The results are verified against NCEP SST analysis for the period of the model integration. The best agreement was seen over the western equatorial Pacific.

The initial analysis of the model output has suggested that the warm pool SST is derived mainly by three important types of oscillations, namely, semiannual, 10–25-, and 30–60-day oscillations. Further examination using Butterworth bandpass filter and EOF analysis has revealed that the tendency of solar radiation is the primary cause of the high-frequency oscillations (20–25 and 30–60 day) and secondary cause for the low-frequency oscillations. Moreover, the evaporative cooling is found to be the primary cause of the low-frequency oscillations and secondary cause for the high-frequency oscillations. The variations of these two forcings were found to be strongly related to convective activities. At high frequencies, convective activities are associated with equatorial waves, whereas at low frequencies such conditions are derived by the migration of the ITCZ.

In relation to the atmospheric moisture content, it was found that the cloud shortwave forcing plays the most crucial role in the solar radiation. The connection between convective activities and the changes in the evaporative cooling is found to be through the humidity deficit at low-frequency oscillations and surface wind speed at high-frequency oscillations. A careful examination of the SST–convection interaction has revealed that the warm pool SST may have an upper limit as suggested by earlier authors.

## 1. Introduction

The tropical atmosphere over the western equatorial Pacific (warm pool) manifests continuous disturbances together with highly active air–sea interaction. Yet, the warm pool SST-(a list of acronyms appears in Table 1) as compared to that of the other sections of the tropical Pacific displays very small spatial and temporal variations. To illustrate the temporal variations, the area-averaged SST is plotted for six consecutive years (1993–99) over the eastern, western, and entire equatorial Pacific in Fig. 1. These time series are calculated from the NCEP SST analysis (more information on this data will be given in section 1). As seen from this figure, the time variation of the area-averaged SST is much greater in the eastern sector. Furthermore, the time series for the eastern sector and the entire tropical Pacific are closely related in terms of their annual variations. The western counterpart, however, displays very different variations.

Another interesting aspect of the western equatorial Pacific is that it is not largely affected by the extreme anomalies such as the ENSO cycle (see year 1997 in Fig. 1). Furthermore, the western Pacific has the warmest SSTs over the entire equatorial Pacific. Even though this is true, observations have shown that the maximum SST in the western Pacific never exceeds around 32°C. All these suggest that the western Pacific SST is driven by a unique mechanism as compared to the rest of the tropical Pacific. This persistent behavior of the western equatorial Pacific has prompted a lot of interesting debates during the last decade on whether or not the SST over this region is regulated. One of the most interesting conclusions from these debates was the relation between convection and SST. Using observational data, earlier studies (see, e.g., Krueger and Gray 1969; Gadgil et al. 1984; Graham and Barnett 1987; Waliser and Graham 1993; Waliser 1996; Lau et al. 1997) have demonstrated that scatterplots of convection (represented by OLR or cloudiness) versus SST display three different regimes. The first regime occurs when the SST is lower than about 27°C; it is characterized by little or no convection. The second regime is when SST is roughly between 27° and 29°C. This area is characterized by vigorous convection. This area is followed by the third regime when

*Corresponding author address:* Nihat Cubukcu, Dept. of Meteorology, The Florida State University, 411 Love Building, Tallahassee, FL 32306.
E-mail: nihat@io.met.fsu.edu

TABLE 1. The list of acronyms used in the text.

| Acronym | Definition |
|---|---|
| BBPF | Butterworth bandpass filter |
| ECMWF | European Centre for Medium-Range Weather Forecasts |
| CEPEX | Central Equatorial Pacific Experiment |
| EOF | Empirical orthogonal function |
| FSUCGSM | Florida State University Coupled Global Spectral Model |
| FSUGSM | Florida State University Global Spectral Model |
| GCM | General circulation model |
| GLAS | Goddard Laboratory for Atmospheric Sciences |
| ITCZ | Intertropical convergence zone |
| NCEP | National Centers for Environmental Prediction |
| MJO | Madden–Julian oscillation |
| MPI | Max-Planck-Institut für Meteorologie |
| OLR | Outgoing longwave radiation |
| PBL | Planetary boundary layer |
| PC | Principal component |
| PCA | Principal component analysis |
| pdf | Probability distribution function |
| ppt | Parts per thousand |
| SST | Sea Surface Temperature |
| TOA | Top of the Atmosphere |
| TOGA | Tropical Ocean Global Atmosphere |
| COARE | Coupled Ocean–Atmosphere Response Experiment |
| UCLA | University of California, Los Angeles |

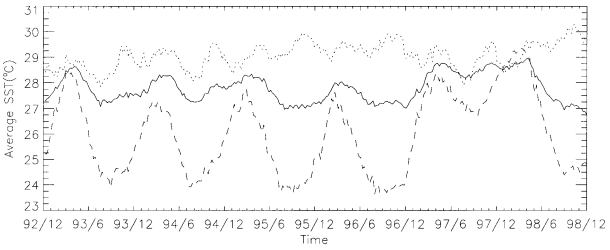


FIG. 1. Time series (from 1993 to 1998) of the SSTs averaged over the areas between ±10° and 125°–150°E, 110°–85°W and 125°E–85°W denoting western (dotted), eastern (dashed), and entire equatorial Pacific (solid), respectively.

SST is over 29°C. In this regimes, the convective measures display a sharp decline.

Although the relationship between tropical SST and large-scale/local convective processes implies a clear role of convection in SST regulation, it does not explain the way this mechanism operates. The first idea toward this came from Graham and Barnett (1987) who argued that the cloud cover associated with deep convection may block some incoming solar radiation and thereby limit the SST. Their analysis was based on the SST–convection relation and an idealized surface heat balance model. Then, Ramanathan and Collins (1991) proposed the so-called thermostat hypothesis to explain the mechanism regulating maximum SST in the warm pool. This theory works in two stages; first, in the presence of convective clouds and high SST, the greenhouse effect results in uncontrolled warming. Second, the highly reflective clouds, as a result of the convection, shield the surface against solar radiation and inhibit the further warming. Wallace (1992) on the other hand, has proposed the following explanation; high SSTs destabilize the atmosphere by heating the planetary boundary layer through surface heat fluxes. In response, the atmosphere stabilizes itself by convection that carries the heat away from the boundary layer. Throughout this process, the latent heat flux is the major factor transporting heat from the ocean to the atmospheric boundary layer. According to Wallace, this stabilization process, with other elements of atmosphere–ocean interaction, is enough to control maximum SST over hot spots such as the warm pool region. A similar explanation was later proposed by Waliser and Graham (1993). They suggested that the convective systems over the Tropics act to stabilize the tropical troposphere that is heated and supplied with the moisture from the ocean surface below by cooling and drying the lower levels and warming and moistening the upper levels.

These important findings have strengthened the hypothesis of a regulated SST in the western tropical Pacific. However, it was realized that the available observations were not sufficient to unveil the regulation mechanism. A complete budget analysis of the warm pool SST is necessary to construct the dynamical and physical aspects of this regulation. Hartman and Michelsen (1993) took the first step toward this when they studied each term in the surface energy balance and their sensitivities to SST using observations and a simple numerical model. Their result displayed that the solar heating and latent heat cooling of the surface are the major contributors to SST. They also indicated that shortwave cloud forcing is more sensitive to the SST gradient rather than the absolute value of SST, implying a large-scale signature in the regulation of SST over the warm pool. This was also the point where the thermostat hypothesis was criticized by Lau et al. (1994). They argued that the cloud changes strongly depend on the large-scale processes that are derived by the complex large-scale atmosphere–ocean circulation as opposed to the local convection.

The studies mentioned above suggest a timescale of the variability of SST that is closely related to that of convection. However, Arking and Ziskin (1994) used three different datasets to show that the variability of the warm pool SST is season- and latitude-dominated. Another result from this study was that cloud effect on longwave radiation is as important as that on solar radiation, which means it is unlikely that clouds have a regulatory effect on SST.

Dominance of seasonal variability of SST was also shown by Zhang and McPhaden (1995) in the western Pacific. They indicated that the seasonal variabilities of SST and the latent heat flux are out of phase and dominated by the surface wind changes, mainly derived by the large-scale atmospheric circulation in this timescale. According to Zhang and McPhaden, the seasonal variability of surface wind overcomes that of the humidity difference between the surface and a reference level, keeps the latent heat flux small, and lets the SST increase with solar radiation. These results

have been confirmed by Zhang et al. (1995) where they pointed out that on the climate timescale, the variation of the latent heat flux at high temperatures is dominated by a variation in wind speed and, therefore, decrease in wind speed leads to a relatively suppressed latent heat flux at high SSTs.

These findings indicate that SST regulation over the western Pacific is an intricate temporal-and spatial-dependent phenomenon. Zhang et al. suggested a simple explanation stating that the climatological mechanisms are the dominant factors maintaining capped SST over the western Pacific. A later study by Lau and Sui (1997) suggested that on timescales of weeks to months over the warm pool, the SST is mainly regulated by the MJO through induced surface fluxes and upper-ocean processes. However, they also argued that the MJO itself is subject to the climatological changes. Sud et al. (1999) claimed that the downdraft during the convective phase of the MJO is a major factor in determining the warm pool SST. They claimed that the descending warm and dry air associated with the downdraft causes the abrupt increase in the surface latent and sensible heat fluxes and thereby begins to cool the ocean surface. According to them, the sudden increase in the surface heat fluxes act as a thermostat analogous to the one proposed by Ramanathan and Collins (1991) except that here, the thermostat is the surface flux and not the shortwave cloud forcing. A recent study by Tian et al. (2001) presents very detailed analysis of the warm pool atmosphere during TOGA COARE and CEPEX. They were able to show that the cloud radiative forcing has a dipole effect on the SST very much resembling the thermostat hypothesis.

In all of these studies mentioned above, the elements that are thought to be responsible in regulating the warm pool SST are usually the atmospheric parameters that are not unilaterally agreed to be the prime factor. The effect of oceanic processes in the regulation of the warm pool SST is not clearly understood and therefore, neglected in most of the studies. An important consensus was that this regulation mechanism could be explained better if each term in the balance equation is examined at each individual timescale with the use of a detailed coupled atmosphere–ocean model. In fact, Lau et al. (1997) stressed the necessity of such detailed work in order to understand the real nature of this regulation phenomenon.

Even though some of the past studies have benefited from simple numerical models (see, e.g., Hartman and Michelsen 1993; Zhang et al. 1995), lack of coupling and simplistic approaches used have made their results hardly convincing. Probably the first coupled numerical study for studying the warm pool SST came by Schneider et al. (1996) who used MPI's coupled GCM. However, they only focused on seasonal variations. Observations in and around the warm pool region were the primary source for the earlier studies and revealed significant amounts of information. However, long discontinuities in the temporal and spatial distributions proved extremely hard to cope with. Lau et al. (1997) also pointed out that the limited amount of observations can sometimes be misleading and therefore, should be used with extreme caution. Remarkably, after reprocessing the OLR–SST relationship, they showed that the third region in the scatterplots of SST versus convection (as explained before) does not really exist in the warm pool region.

Our goal in this paper is to ease the problems mentioned above and perform a residue-free thermodynamic budget of the coupled system by utilizing the FSUCGSM to assess the contributions from each term in the sea surface temperature equation. Global atmospheric analysis from ECMWF and global SST analysis from NCEP (R. Reynolds, D. Stokes, and T. Smith, personal communication) are used as initial conditions for the atmospheric model. The initial conditions for the ocean model are obtained at the end of a 10-yr spinup period. Levitus climatology (Levitus 1982) is used to initiate the spinup processes. The resulting initial state for the coupled model reflects the actual atmospheric and oceanic conditions for the initial time (we have chosen 3 March 2001 as the starting date). More information on ocean spinup processes can be found in LaRow and Krishnamurti (1998). To obtain a residue-free SST simulation, the coupled model is redesigned in a way that all the numerical interventions such as filtering, nudging, etc., are reduced to a minimal level.

## 2. Methodology

SST equation as defined in FSUCGSM can be written as

$$\frac{\partial T}{\partial t} = -\mathbf{V}\cdot\boldsymbol{\nabla}T - w\frac{\partial T}{\partial z} + \frac{\partial}{\partial z}\left(D_v\frac{\partial T}{\partial z}\right) + D_H\nabla^2 T + F, \tag{1}$$

where $\mathbf{V}$ is the horizontal velocity, $w$ is the vertical velocity, and $D_H$ and $D_v$ are horizontal and vertical diffusion coefficients, respectively. The surface forcing $F$ can actually be decomposed into the following components:

$$F = \frac{1}{\rho_0 C}\frac{\partial}{\partial z}(Q_s - Q_t - Q_e - Q_H), \tag{2}$$

where $C$ is the specific heat for the ocean and $\rho_0$ is the density of the water. The terms in the parentheses from left to right represents solar, terrestrial, evaporative, and sensible heat fluxes, respectively. Now, it can be seen that the SST tendency in Eq. (1) is made up of eight partial tendencies, namely, shortwave, longwave, latent heat, sensible heat, horizontal advection, vertical advection, horizontal diffusion, and vertical diffusion. Since all of these appear in Eq. (1), thereafter, they will be referred as direct contributions. The first four of these

contributions are the direct outcome of air–sea interaction, whereas all the others are involved with the oceanic processes that may indirectly be linked to the air–sea interaction due to momentum transport into the ocean. There is one additional widely used term, which is the convective adjustment resulting from numerical representations. This term is considered as a direct contribution since it is applied to the vertical temperature profile in the ocean at each time integration.

Any variable that is used in calculation of the direct contribution will be referred as indirect contribution. Surface wind speed, cloud cover, etc., are, for example, some of the indirect contributions. To obtain a residue-free analysis, it is important that Eq. (1), after adding convective adjustment, leave very small residue during the time integration of the coupled model. For this reason, the FSUCGSM is redesigned to produce a very small residue up to order of $10^{-13}$°C day$^{-1}$ as shown in Cubukcu (2001).

The entire context of this project is based on the 1-yr numerical integration of the redesigned FSUCGSM, from March 1996 to March 1997 (the date is chosen arbitrarily). An area-averaged time series for each direct contribution is derived from the numerical integration. Area averaging for the warm pool domain is done on an area between ±10° latitude and between 125° and 150°E longitude. Unless otherwise stated, this area will be called the warm pool, or, interchangeably, as the western equatorial Pacific. The land points in the warm pool region are excluded from the calculations. When preparing the time series, each term is taken as it appears in Eq. (1). Since we will mostly be working with the anomaly fields, it should be noted that for a term that is always negative (such as the latent heat term) negative/positive anomalies denote more/less cooling.

As part of the residue-free analysis, we first obtain the power spectrum of a 1-yr-long record for the warm pool SST. Based on this spectrum, the most important harmonics are identified. Then, using the bandpass-filtering technique, the time series of each term is filtered for each important timescale. Next, the filtered time series are used to explore the primary forcing(s) on the warm pool SST for each timescale. This part is accomplished using PCA analysis. All this information is then used in order to explore the regulation mechanism of the warm pool SST.

## 3. Numerical model

### a. Ocean model

The ocean model employed in here is a modified version of a Max Planck Institute ocean model (Sterl 1991; Latif et al. 1994). The model has 17 irregularly spaced vertical layers. The upper part of the ocean is given more attention because turbulent activities due to external forcing are effective there. Therefore, the first 300 m have finer vertical resolution. The thickness of the layers from the top is 20, 20, 20, 20, 20, 30, 30, 40, 50, 50, 100, 200, 500, 1000, 1500, and 2000 m, respectively. We have variable resolution in the meridional direction where within ±10° of the equator the resolution is constant at 0.5°, between ±10° and ±20° it increases to 1° and it is 5° outside of ±20°. Constant resolution of 5° is used in the zonal direction. The equations of motion are solved using finite differencing techniques on a horizontally staggered E-grid scheme (Arakawa and Lamb 1977).

The time integration of the full system with the time step of 120 min is carried out by the method of fractional steps. This method allows for each individual equation to be separated into components that are integrated individually and then combined to give the solution of the full system.

For turbulent diffusion, a constant mixing coefficient of 1000 m$^2$ s$^{-1}$ is used in order to calculate the horizontal mixing processes, whereas in the vertical a Richardson number–dependent (Ri) formula is used. Surface forcing is represented by the exchange of heat and momentum at the air–sea interface.

### b. Atmospheric model

The numerical weather prediction model used in this study is the FSUGSM described in Krishnamurti et al. (1998). The horizontal and vertical resolutions of the model are flexible; for this study we use a horizontal resolution truncated at wavenumber 42 (T42), which gives the approximate grid mesh of 2.8° latitude and a vertical resolution of roughly 0.5 km described by 14 $\sigma$ levels between roughly 50 and 1000 hPa. Here $\sigma = p/p_s$, where $p$ is the pressure at a level and $p_s$ is the surface pressure. A semi-implicit time integration scheme is used with the time step of 20 min to represent the time derivatives in the model equations. The high-frequency gravity wave oscillations are suppressed by the semi-implicit time differencing wherever these waves appear in the model equations. The initial data sources for FSUGSM are the global analysis of ECMWF and the sea surface temperatures from NCEP.

The prognostic model variables are vorticity, divergence, dewpoint depression, surface pressure, and a variable that combines the geopotential height and logarithm of the surface pressure. The model physics include the following:

- modified Kuo scheme for cumulus parameterization (Krishnamurti et al. 1983);
- shallow convective adjustment (Tiedke 1984);
- dry convective adjustment;
- large-scale condensation;
- planetary boundary layer parameterization by similarity theory (Businger et al. 1971);
- parameterization of shortwave by Lacis and Hansen

(1974) and longwave by Harshvardhan and Corsetti (1984).

## 4. Verification

In this section, the validation and verification of the predicted SST with NCEP SST are discussed. The coupled model has previously been applied to numerous climatological problems (see, e.g., LaRow and Krishnamurti 1998; Krishnamurti et al. 2000). The results have proven that the FSUCGSM is an excellent tool for climatological studies. Based on previous successes of this model, we assume that all direct and indirect contributions to SST are reasonably simulated provided that the SST agrees well with the observations. It is hard to perform verification of each forcing in the SST equation due to the lack of available observational data consisting of the same spatial and temporal characteristics. Figure 2 shows the differences (model − observed) in the seasonal mean SST fields for one year of model integration.

Overall, this figure shows that the comparison of the model results to NCEP analysis displays good agreement in most of the equatorial Pacific. There are some discrepancies in the eastern equatorial Pacific in the region of the cold tongue and also in the downstream parts of the California and Peru Currents as also noted in Latif et al. (1994). These discrepancies are due to inadequate simulation of the narrow canal coastal currents such as those off the coasts of California and Peru and thereby the strong coastal upwelling in these regions. Also, the resolution and the interpolation routines used in the model and those used in the NCEP analysis often cause large differences during the comparison. The comparison in the western Pacific, which is the main focus of this study, is very encouraging.

Time variations of the weekly mean model and NCEP SSTs are shown in Fig. 3 for the western, eastern, and entire equatorial Pacific regions. The sampling period is taken as one week to be consistent with NCEP's weekly analysis. It is again clear that the model performs well especially in the warm pool region for the entire period of the integration. The warm pool region has marked intraseasonal variations in both the observed and the predicted time series. These variations were also noted by Lau and Sui (1997) using observations during TOGA COARE. In the longer timescale, both the model-predicted SST and the NCEP analysis display semiannual variation in the western equatorial Pacific. Although the model simulation displays similar low-frequency variation in the eastern Pacific, the analysis shows a seasonal type of variation. Our simulation did not capture this shift at low frequencies as one goes from west to east. Both the semiannual and annual variations are associated with the annual march of the ITCZ. Observations shows that the ITCZ usually stays around 10°N in the eastern Pacific (Waliser and Gautier 1993). In fact, if that was the case in the model simulation, the time series of the SST would have had seasonal variations instead of semiannual type of variations. The model fails to capture this, probably due to same reasons we mentioned above for the spatial comparison.

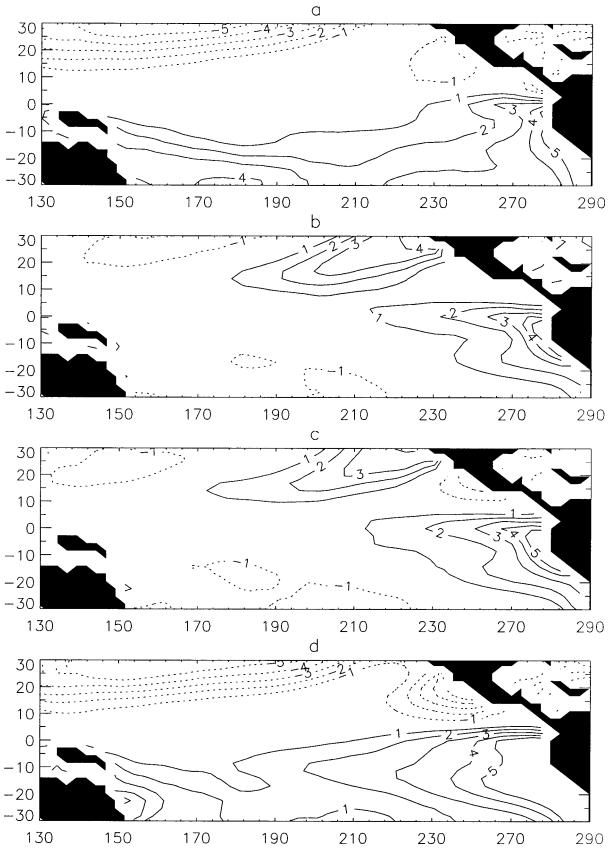


FIG. 2. Seasonal mean SST (model − observed); (a) spring 1996, (b) summer 1996, (c) fall 1996, and (d) winter 1996/97. The land–sea mask array of FSUCGSM is used to plot the continents. The contour interval is 1°C.

The comparison for the entire tropical Pacific, however, indicates that excluding the coastal features in the eastern Pacific, the FSUCGSM captures a great portion of the temporal and spatial variations of the equatorial Pacific SST on an annual timescale. Errors associated with the coastal features in the eastern Pacific can be assumed to have little effect on the entire equatorial Pacific SST, especially in the western end. Thus, FSUCGSM can be a very useful tool for studying the mechanism of the warm pool SST.

## 5. Residue-free budget analysis of the warm pool SST

In this section, the types of variations existing in the warm pool SST are investigated using area-averaged time series. For this goal, we have first computed the power spectrum of the warm pool SST for the time period defined in the introduction. The power spectrum is displayed in Fig. 4. Instead of using the conventional

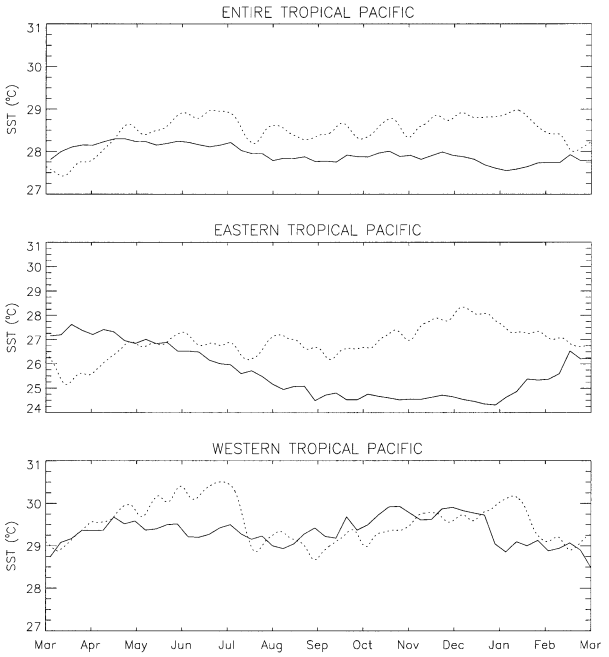


FIG. 3. Comparison between the model (dotted) and NCEP (solid) weekly mean SSTs averaged over different sections of the equatorial Pacific as shown at the top of each panel. The length of the time integration is 1 yr starting from 1 Mar 1996. The labels on the abscissa are placed at the first day of each month.

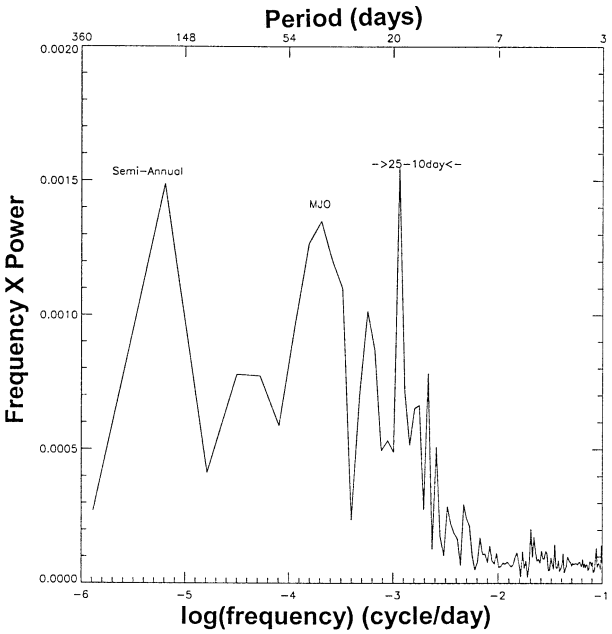


FIG. 4. Power spectrum of the area-averaged warm pool SST for the time period defined in the introduction. The area-conserved transformation on $x$ and $y$ axis provides a better look in both time and frequency domain as discussed in Zangvil (1975).

frequency–power relationship, we have made an area-conserving transformation in order to have a better look. The new sketch of the variables [frequency $\times$ power vs log(frequency)] provides consistency between the variations in the time and frequency domains. This technique was first used by Zangvil (1975) and is still being used in numerous meteorological applications. As shown in Fig. 4 it suggests that by the nature of the spectrum and earlier observational studies (see, e.g., Lau and Sui 1997), it may be possible to partition the spectrum into three distinct regions. The first region is where the spectrum has a peak at around 180 days. This suggests the existence of a semiannual variation of the warm pool SST. The semiannual variation is associated with the annual variation of the solar radiation. The second region in the spectrum marked as MJO falls roughly into the 30–60-day band. The variation of the warm pool SST on this timescale contains a great portion of the total variance, as it was the case for the semiannual variation. MJO can be regarded as a baroclinic wave disturbance originating over the Indian Ocean and traveling eastward around the globe (Madden and Julian 1971, 1972; Krishnamurti and Gadgil 1985). The most intense phase of these oscillations occurs over the tropical Indian Ocean and over the warm pool region. Atmospheric conditions associated with MJO change drastically. The wet phases of these oscillations are characterized by heavy convection, often with westerly wind anomalies, whereas the dry phases of these oscillations are characterized by clear and dry air with easterly wind anomalies (Knox and Halpern 1982; McPhaden and Taft 1988; Fasullo and Webster 2000). The SST responds to these atmospheric variations through air–sea interaction. The third region is the 10–25-day band. Lau et al. (1997) described these as biweekly oscillations created by the local synoptic events regardless of the wet/dry phases of MJO. In a more recent paper by Fasullo and Webster (2000), it was argued that these oscillations are associated with the Kelvin waves that are believed to be ignited by the westerly wind bursts. The dynamical aspect of these oscillations is quite similar to that of MJO, except that their impact on atmospheric and oceanic variables is smaller compared to that of MJO. These disturbances also comprise wet/dry phases associated with the westerly/easterly wind anomalies. Even though there are notable similarities between MJO and the 10–25-day oscillations, there is no clear indication that these variations are related.

The possible regulation mechanism for the warm pool SST needs to be explored at each of these individual timescales. This isolation is necessary because there is no apparent relation among these distinct variations. After separating each timescale, the direct contributor(s) acting on the SST can be evaluated without facing the contamination problem from other types of variations. Once these contributors for each type of variation are determined, we can then seek what determines their variations using related atmospheric and oceanic variables previously named as indirect contributions. The use of a bandpass filter combined with the principal component

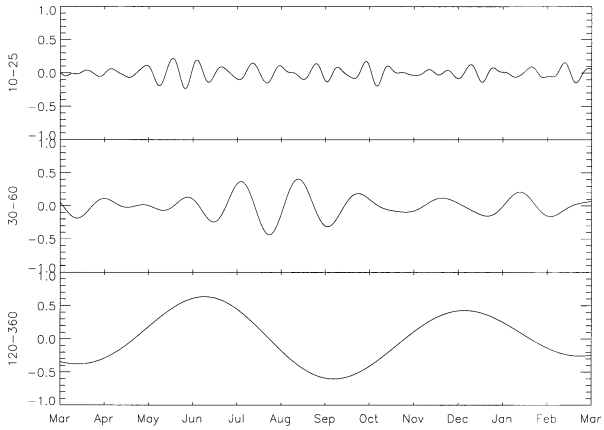


FIG. 5. Filtered time series of the area-averaged warm pool SST in °C. The annual mean is removed before applying the bandpass filter. The bandwidth for each plot is displayed on the ordinate in days. These bands are found to be the most important timescales in which the warm pool SST displays large variations as seen in Fig. 4.

analysis may be an excellent tool to reach this goal. The layout for this plan is as follows.

1) Use a bandpass filter for the timescales described above to obtain the filtered time series of the direct contributions.
2) Apply PCA (EOF analysis) to the time series obtained in the previous step.
3) Obtain the most representative contributor(s) using the information gathered from the principal components and corresponding variances.

Using a bandpass filter allows us to focus on a single type of variation. The principal components calculated using the filtered time series do not provide temporal information. Instead, each principal component mimics one or a combination of the direct contributions. Thus, by comparing the variations of the principal components with those of the direct contributions, dominant terms in the SST equation can be determined. The same conclusion can be obtained if the EOF analysis is applied to the raw time series and then the principal components are filtered. However, it would then be difficult to partition the percent variances among the major forcings.

For the first step, BBPF is used. This filter has been employed extensively in meteorological applications (see, e.g., Murakami 1979; Krishnamurti and Subrahmanyan 1982). Only the time series of shortwave, longwave, latent heat, sensible heat, total advection, vertical diffusion, and convective adjustment are filtered, along with the SST tendency. The covariance matrix used in the EOF analysis is constructed by placing these contributors at each row in the order listed above following the columns corresponding to the time levels.

BBPF is first applied to the time series of the warm pool SST for the frequency bands mentioned in the previous section. The resulting filtered time series are displayed in Fig. 5. In relation to the spectrum of the warm

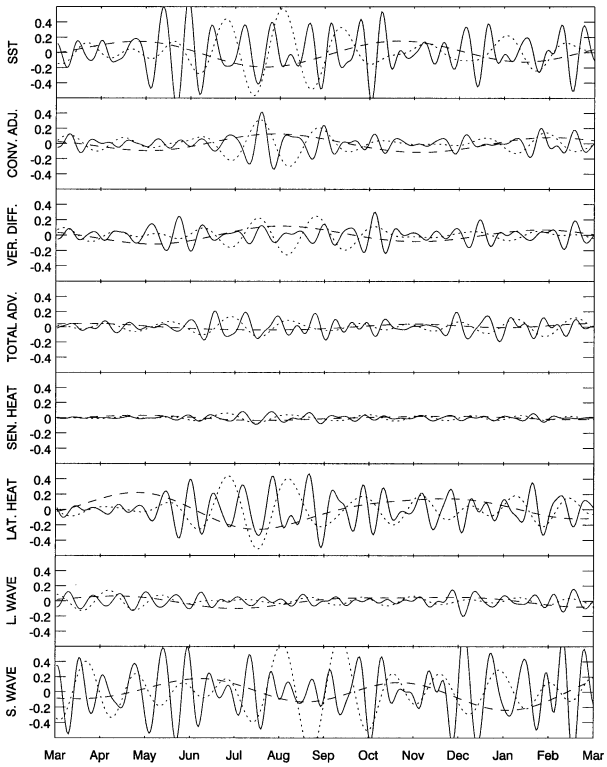


FIG. 6. The filtered time series of the direct contributions and SST tendency averaged over the warm pool region for 10–25- (solid), 30–60- (dotted), and 120–360-day (dashed) bands. The scales on the ordinate axis are kept the same for all contributors in order to present a comparative representation. The units are in °C day$^{-1}$. The sum of all contributions is the net tendency displayed at the top. The time integration period is defined in the introduction.

pool SST in Fig. 4, this figure clearly displays that the variation of the warm pool SST is inversely proportional to the frequency, that is, the largest deviations from the annual mean occurs at the low frequencies and the smallest variations occur at the high frequencies. The dominance of the low-frequency variations was also pointed out by many authors (see, e.g., Arking and Ziskin 1994; Zhang and McPhaden 1995) using various kinds of observational data over the warm pool domain. Furthermore, the comparison between the 30–60- and the 10–25-day variations is also consistent with the observational findings (Fasullo and Webster 2000). We now feel very confident that the FSUCGSM not only successfully simulates the types of variations in the warm pool SST, but also captures the relative importance of each timescale.

Considering that area-averaged quantities are used for this analysis, it is realized that the warm pool SST undergoes substantial changes. Therefore, in the following discussion, considerable effort is made to investigate all these variations. Figure 6 displays the filtered time series of the direct contributions and the tendency of the warm pool SST for 10–25-, 30–60-, and 120–360-day variations. This figure is the basis of the entire EOF analysis.

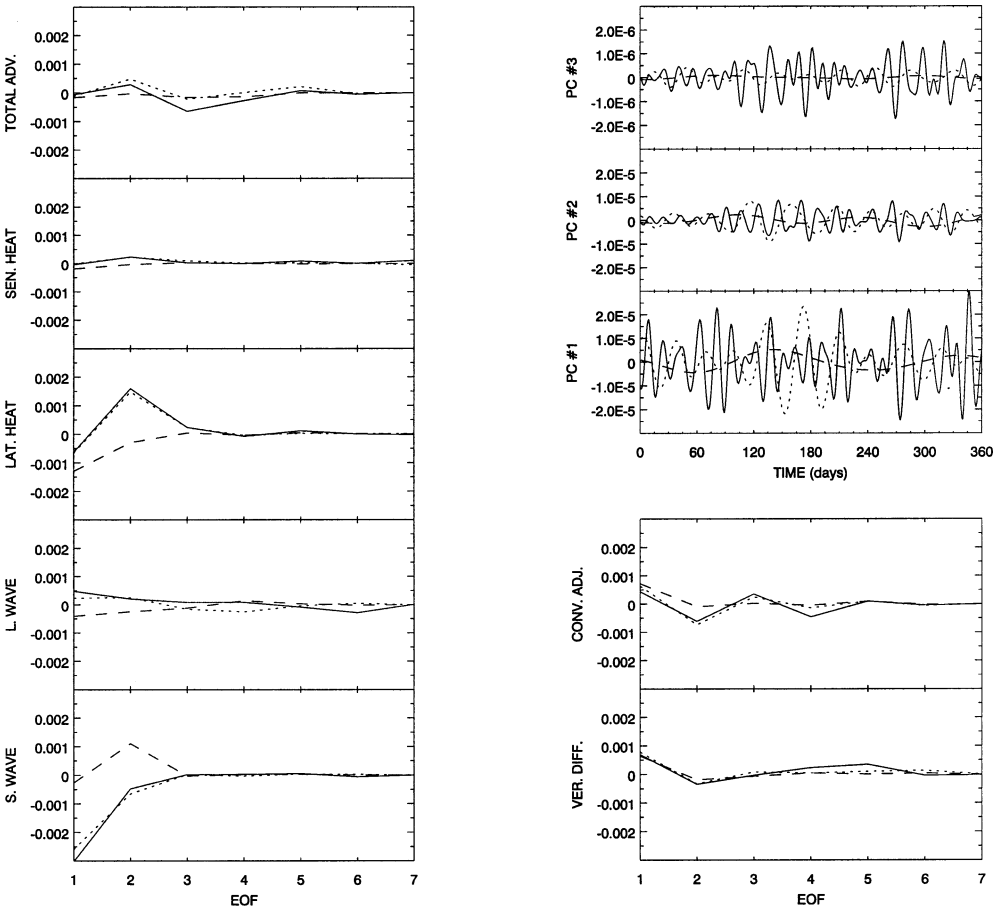


FIG. 7. EOF analysis of direct contributions of SST in the warm pool region. Each line style denotes a different timescale as defined in Fig. 6. Time series used here are also those in Fig. 6. (left), (bottom right) The magnitude vs EOF number for each tendency. (top right) First three principal components.

The results of EOF analysis for the direct contributions are displayed in Fig. 7 and Table 2. Starting with the 10–25-day variations, the results can be interpreted as follows. The first (largest) eigenvector corresponding to the first (largest) eigenvalue belongs to the shortwave contribution. All other first eigenvectors are less than around one-third of the eigenvector that belongs to the shortwave contribution. The first principal component contains 66% of the total variance. This is to say that the shortwave contribution is the quantity most heavily altered by the 10–25-day oscillations. The second largest eigenvalue in Table 2 corresponds to the second largest eigenvector associated with the latent heat term. The second principal component contains roughly 24% of total variance. Together, the first two principal components contain about 90% of the total variance. With this information at hand, one can easily assume that the shortwave and, secondarily, the latent heat term, can explain the 10–25-day variations seen in the evolution of the warm pool SST. Since the temporal variation is

TABLE 2. Eigenvalues and percent variances of the direct contributions of the warm pool SST. The values are shown in decreasing order.

| Semiannual | | Madden–Julian | | 10–25 day | |
|---|---|---|---|---|---|
| Eigenvalue | Variance (%) | Eigenvalue | Variance (%) | Eigenvalue | Variance (%) |
| $2.16 \times 10^{-6}$ | 67.4 | $6.28 \times 10^{-6}$ | 67.1 | $8.84 \times 10^{-6}$ | 66.0 |
| $9.80 \times 10^{-7}$ | 30.6 | $2.67 \times 10^{-6}$ | 28.5 | $3.26 \times 10^{-6}$ | 24.4 |
| $3.76 \times 10^{-8}$ | 1.2 | $2.20 \times 10^{-6}$ | 2.4 | $7.01 \times 10^{-7}$ | 5.2 |
| $1.84 \times 10^{-8}$ | 0.6 | $1.15 \times 10^{-7}$ | 1.2 | $3.55 \times 10^{-7}$ | 2.7 |
| $6.06 \times 10^{-9}$ | 0.2 | $5.42 \times 10^{-8}$ | 0.6 | $1.40 \times 10^{-7}$ | 1.0 |
| $6.50 \times 10^{-10}$ | 0.0 | $2.13 \times 10^{-8}$ | 0.2 | $8.16 \times 10^{-8}$ | 0.6 |
| $3.50 \times 10^{-11}$ | 0.0 | $2.38 \times 10^{-9}$ | 0.0 | $1.04 \times 10^{-8}$ | 0.1 |

fixed using the bandpass filter, the PCs should imitate the dominant terms in SST equation.

Similar analysis is also applied to the 30–60-day timescale. It is seen that the shortwave term contains most of the variance (about 67% of total variance). The first principal component shows a lot of similarity to the filtered SST tendency in Fig. 6. Nevertheless, the 28% variance in the second PC is important to consider. By comparing the second EOFs, one can easily say that the variations of the latent heat contributions are responsible for this portion of the total variance. Together, the first and second PCs contain about 97% of the total variance and thus, they undoubtedly dominate the MJO oscillations in the variation of the warm pool SST.

The analysis of the semiannual cycle is also displayed in Fig. 7 and Table 2. For this case, the bandpass filter covers the range between 120- and 360-day periods. The PCA results reveal that the main driving force behind the semiannual cycle of SST is now the latent heat term as can be inferred from the EOF plots. The first principal component contains about 67% of the total variance. This is followed by the shortwave contribution with a partial variance of 30.6. Similar to the 10–25- and the 30–60-day oscillations, both evaporative and shortwave fluxes contain almost the entire variance of the semiannual oscillations. The dominance of the latent heat term in the seasonal timescale was also pointed out by Zhang and McPhaden (1995) using observations.

In summary, it is concluded that the variations of the warm pool SST discussed above, appear to arise primarily as a result of air–sea interaction. Among the surface forcing terms, the shortwave and latent heat terms are the primary forcings on the warm pool SST. For the timescales extending from 10–25 to 30–60 days, the shortwave contribution is found to be the primarily important, and the evaporative contribution is found to be a secondarily important factor. However, as the timescale becomes longer, the evaporative contribution becomes more important than the shortwave contribution. In relation with these findings, one can argue that there is a mutual cancellation between shortwave and evaporative flux contributions in timescales roughly between 60 and 120 days. As seen in the spectrum of the warm pool SST in Fig. 4, this results in very small variations on such timescales.

Knowing the importance of these terms is the first important step to unveil the possible regulation of the warm pool SST. Yet, we still have to establish physical and dynamical reasoning of the variations. For this, each contribution to the shortwave and latent heat term ought to be examined. These were previously defined as indirect contributions. In the next two sections, this issue will be investigated thoroughly. The outcome of this investigation and the results discussed above will be used to construct the regulation mechanism of the warm pool SST.

## 6. The elements of the evaporative flux contribution

As described in the previous section, the evaporative fluxes are the main factor determining the warm pool SST at the semiannual timescale and is secondarily important at shorter timescales. One major result that may be derived from this is that the direct response to the annual cycle of the incident solar radiation does not entirely work over the western Pacific. Since the evaporative flux term was found to be the primary contributor in this timescale, it becomes natural to seek similar semiannual variations in its contributors. In this way, it is possible to find the very first element that carries the semiannual oscillation. The evaporative flux in FSUCGSM is defined as

$$Q_e = \rho L C_E u_a \Delta q, \tag{3}$$

where $u_a$ is the surface wind, $\Delta q = q_0 - q_a$ is the moisture deficit where $q_0$, $q_a$ are the surface and reference level specific humidity, respectively, and $C_E$ is the stability-dependent bulk coefficient. The variations in the bulk coefficient are usually neglected (see, e.g., Zhang and McPhaden 1995). Similarly, our results indicate that the semiannual variations of bulk exchange coefficients are about 3 orders of magnitude smaller than those of surface wind speed and humidity deficit. Therefore, for the sake of simplicity, it is assumed that these coefficients remain constant throughout the time integration. Then, only the time evolution of the surface wind speed and moisture deficit should be enough to explain the semiannual variation in the evaporative fluxes and thereby in the warm pool SST. The individual contributions from the surface wind and humidity deficit, however, are not straightforward to obtain, since Eq. (3) is not a linear equation. Using simple perturbation technique, the linearized contributions of the surface wind and moisture deficit can be obtained as

$$Q'_e = \rho_0 L C_E (\overline{u_a} \Delta q' + u'_a \overline{\Delta q}), \tag{4}$$

where the bars and primes denote the mean and perturbed states, respectively. In addition to $C_E$, we also assumed that $\rho_0$ is constant. The first term on the right-hand side is the contribution from the moisture deficit and the second term is the contribution from the surface wind speed. This new equation enables us to investigate the contributions independently, yet it is only a first-order approximation to the actual relation in Eq. (3). Thus, some caution needs to be exercised when using this method, since it may be misleading in the presence of strong nonlinearity, especially at high frequencies. The following discussions are based one the terms in Eq. (4).

### *a. Semiannual oscillation*

Figure 8 displays the filtered time series of the terms in Eq. (4) along with those of the surface and reference

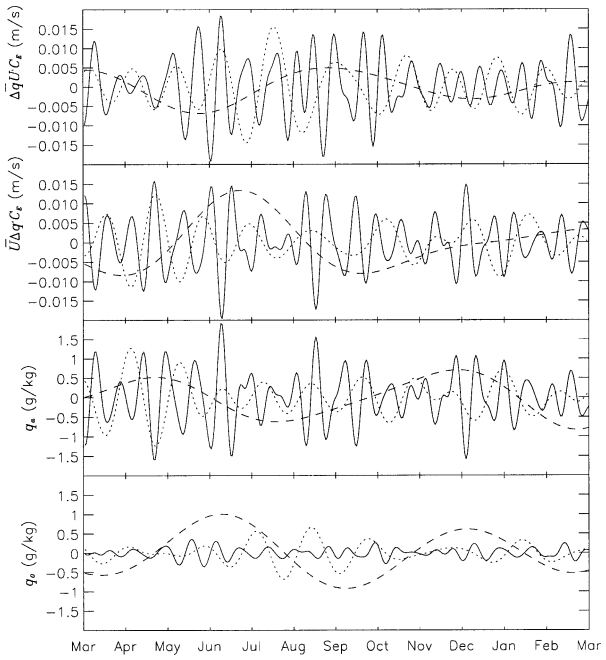


FIG. 8. Bandpass-filtered time series of the surface wind and moisture deficit terms in Eq. (4) along with the surface and reference level specific humidities averaged over the warm pool. The same scale is used for the surface wind and moisture deficit in order to apprehend their contribution to the evaporative flux term. Line styles are defined in Fig. 6. The time integration period is defined in the introduction.

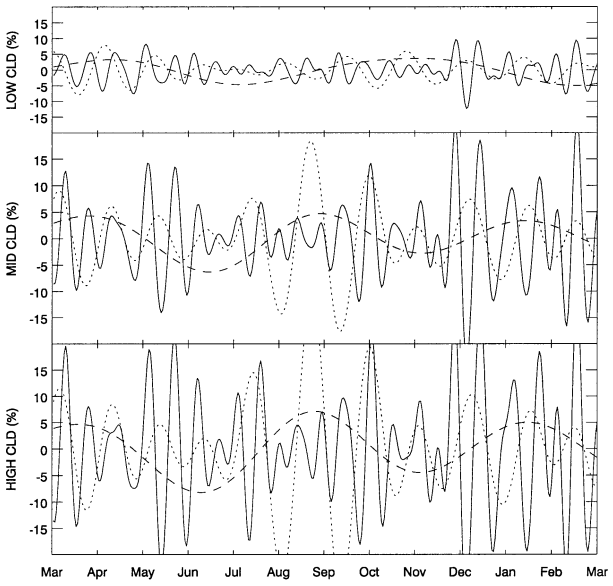


FIG. 9. Time series of the area-averaged cloud cover over the warm pool region. Each line style denotes different timescale as defined in Fig. 6.

level specific humidity. The time series are constructed using area-averaged constituents as done before. For the timescales between 120 and 360 days, it can be argued that the contributions of the evaporative heat flux tend to partially compensate each other. The variations of the humidity deficit are considerably larger than those of the surface wind term. The 1–2-months phase difference between these two terms is what determines the semiannual variation of the evaporative flux contribution. These findings contrast those of Zhang and McPhaden (1995) who used buoy data around 8°N and 165°E for their analysis. They suggested that these slow variations are due to variations in the surface wind speed. Humidity deficit was found to be less important for evaporative fluxes. Our findings indicate that the humidity plays perhaps a more important role, compared to that of the wind speed. Nevertheless, the effect of the surface wind speed is important since it works against the humidity deficit. Their analysis was based on the time series at a single point in the warm pool region due to availability of the data. In contrast, here, area-averaged values over the warm pool region are used. Another important point that can lead to these differences is that it is highly possible that the contaminations from other types of variations, such as MJO or smaller timescale phenomena, are affecting the qualitative interpretations. Zhang and McPhaden used the raw data for their analysis. Therefore, their analysis might carry such contaminations that may be avoided using bandpass-filtered time series. Maybe the most misleading point when comparing the contributions of humidity deficit and surface wind speed to evaporative fluxes is the direct comparison of the variations of the humidity deficit and the surface wind speed. As seen in Eq. (4), the actual contributions to the evaporative fluxes can be approximated by $\overline{u}_a \Delta q'$ and $\Delta \overline{q} u'_a$. Depending on the mean state, the comparison between these terms can be significantly different than the comparison between $\Delta q$ and $u_a$. It is noted that area-averaged $u_a$ used in this discussion is somewhat larger than the surface wind in Zhang and McPhaden (not shown here). It may be possible that the models produce stronger surface wind as compared to observations or the difference is simply due to different averaging procedures. This issue could not be cleared up at this time due to lack of comparative observed fields. Nevertheless, our results indicate that the effect of humidity deficit is not negligible.

Due to its semiannual behavior, the possible cause for these variations could be the migration of the ITCZ, which is the rising branch of Hadley circulations between $\pm 10°$ latitudes. With the help of the observational findings (see, e.g., Newell et al 1972; Waliser and Gautier 1993) it can be easily anticipated that the ITCZ crosses the warm pool domain (see our definition of the warm pool in the introduction) 2 times in a year. This is also clear in Fig. 9, which displays the model-derived area-averaged cloud cover (high, middle, and low) over the warm pool. Together with the observational findings and our analysis here, the semiannual oscillation may be connected to the movement of the ITCZ as follows. Throughout the boreal spring, the ITCZ is right over the warm pool area. During this time period, the evaporative flux contribution in Fig. 6 decreases to its lowest

values. In relation with this, the SST tendency displays an increasing trend. The SST anomalies in Fig. 5 are also at their lowest values during early spring and start to increase for the rest of the season in relation with increasing tendency. The surface wind term in Fig. 8, on the other hand, is constantly decreasing, which is an indication of the low-level convergence zone throughout the spring. The humidity deficit term is at its lowest level causing very little evaporation. These conditions are clear evidence of continuous mixing due to convection associated with the ITCZ. The time lag between time series of the terms in Eq. (4) might be related to the different response time of these two terms to the migration of the ITCZ.

In the boreal summer, the ITCZ is located around 10°–15°N (see Newell et al. 1972; Waliser and Gautier 1993). Decreased amount of cloud cover over the warm pool in Fig. 9 is a clear sign of northerly displacement of the ITCZ. As a result of this, the convective activities are reduced over the warm pool region. The northward shift of the ITCZ lets the low-level flow from the southern high latitudes bring drier air into the warm pool region. This situation results in a high humidity deficit, and since the ITCZ is away from the warm pool region, it also results in increasing surface wind speed. Together, these changes induce larger evaporative fluxes that slow down the increasing trend of the SST and eventually cause it to decrease at the early stages of the boreal autumn. Similarly, changes in autumn and winter seasons can be explained, using the information in Figs. 6 and 8.

As a result, in a 1-yr time period, the evaporative fluxes and thereby the SST over the warm pool display warm/cold phases at every 180 days. The main mechanism causing these changes is the migration of the ITCZ. The response time for each element of the evaporative cooling is different as depicted from the Fig. 8. Therefore, both surface wind and humidity deficit should be considered as important parts of the semiannual variations, even though the humidity deficit displays larger variations.

### *b. 30–60- and 10–25-day oscillations*

Due to extreme resemblance between these two types of oscillations, the discussions are given concurrently. Although the evaporative cooling is not the primary forcing for these timescales, accounting for a partial variance above 20%, it can be influential on the warm pool SST.

As seen in Fig. 8, the variations in the humidity deficit and surface wind for these timescales are almost perfectly out of phase. This efficient neutralization results in minor variations in evaporative fluxes. Recall that at the semiannual timescale, these two terms had much smaller phase shifts that led to substantial variations in the evaporative heat flux term as compared to the other terms in the SST equation. This is clear evidence that the dynamical processes driving the semiannual oscillations differ substantially from those of the 30–60- and 10–25-day oscillations. The semiannual variations are shown to be associated with a thermally driven circulation whereas the high-frequency oscillations are associated with the equatorial baroclinic waves. In any case, resulting convective activities appear to be the main cause behind the variations, but the way the convection is initiated varies substantially between high- and low-frequency oscillations.

Using the cloud cover information in Fig. 9, it can be argued that the convective phase of the high-frequency oscillations is characterized by high evaporative cooling due to positive surface wind anomalies whereas the convective phase of the semiannual oscillation is characterized by decreasing evaporative cooling due to very low-negative humidity deficit anomalies. It appears that the wind-induced cooling is more productive at short timescales, and less at large timescales and vice versa for the cooling by the moisture deficit.

These wavelike disturbances are very similar to those discussed in Fasullo and Webster (2000). They are of result of baroclinic/barotropic instability of the atmosphere. This is true for both the 30–60- and 10–25-day oscillations. The ocean response to these disturbances in terms of the area-averaged fields, such as those used here, is considerably minor as compared to slow variations such as semiannual oscillations.

## 7. The elements of the shortwave contributions

Earlier, we had found three distinct timescales in which the warm pool SST shows marked variations. It was shown that, of these variations, in addition to the diurnal variation, 10–25- and 30–60-day oscillations were primarily functions of shortwave contribution. We now attempt to determine the processes that give rise to these variations. To do that, one has to first establish a clear understanding of the shortwave parameterization in our numerical model. We can divide the parameterization of the shortwave contribution into three different components, namely, $O_3$, clear sky, and cloudy sky contributions as explained in Cubukcu (2001). The influence of $O_3$ absorption is a function of atmospheric moisture content in addition to the model-independent $O_3$ content. Therefore, $O_3$ absorption is calculated for the clear and cloudy air separately.

The second component of the shortwave contribution is the clear-sky absorption. For this part, the effective optical path of the scaled water vapor is the most important component for clear-sky absorption. Here, the term clear sky refers to a nonscattering atmosphere. Therefore, the only source for the clear-sky upward fluxes is the ground reflection. Considering that the albedo of the surface over the tropical Pacific does not change much throughout the year, variations of the clear-sky fluxes can be attributed mostly to those of the optical path.

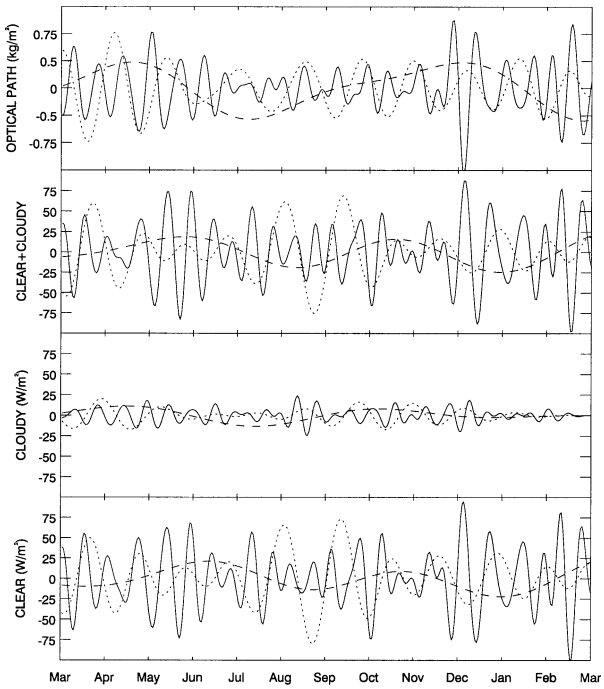


FIG. 10. Bandpass-filtered contributions (clear- and cloudy-sky fluxes) to the tendency of the solar radiation in SST equation along with the sum of these contributions and the optical path of the water vapor averaged over the warm pool region. The optical path of the water vapor is in kg $m^{-2}$ and the fluxes are in W $m^{-2}$. Line styles are defined in Fig. 6. The time integration period is defined in the introduction.

Finally, for the cloudy atmosphere, multiple scattering becomes important. Optical thickness for the cloudy sky is the sum of the optical thickness of clear air and clouds,

$$\delta = \delta_c + k_\nu y, \tag{5}$$

where $\delta c$ is the cloud optical thickness and $k_\nu y$ is the optical thickness of the clear air. In addition to the direct solar radiation, the cloudy sky produces diffuse radiation due to scattering by the cloud droplets. Therefore, for the cloudy sky, the source for the upward solar fluxes is not only the surface reflection but also multiple scattering. The important elements of the diffuse radiation are the phase function and single-scattering albedo assumed to be proportional to the ratio of cloud optical thickness to the total optical thickness. Unlike the clear sky, the cloudy sky can both heat the atmosphere by enhancing the attenuation, and cool the atmosphere by reflecting the radiation back to space. The latter is usually called cloud shortwave forcing. Both cloud shortwave forcing and absorption act to cool the surface by reducing the amount of radiation that reaches the surface.

Using the information given above, it may be assumed that the net solar flux at the surface of the ocean originates from two main components, namely, clear-sky and cloudy-sky fluxes. The $O_3$ absorption may be regarded as an integral part of these components as explained above.

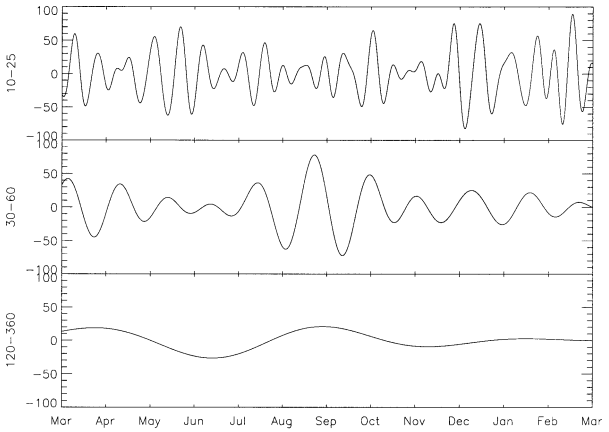


FIG. 11. Bandpass-filtered time series of the upward solar fluxes at TOA. These plots are prepared using the area-averaged values over the warm pool region. The bandwidth for each plot is displayed on the ordinate in days.

### *a. Semiannual oscillations*

The shortwave contribution contains about 30% of the total variance in the semiannual timescale as discussed before. The filtered time series of the clear and cloudy air fluxes together with the optical path is given in Fig. 10. Recall from earlier discussions that the net solar flux at the surface is the exact sum of the indirect contributions, namely, the clear-and cloudy-sky fluxes. This means that going from indirect to direct fluxes, the residue is zero. The net flux is exactly the same as the shortwave contribution in Fig. 6 if converted into the unit °C $day^{-1}$. The optical path is a measure of the moisture content of the atmosphere. Thus, it can be very useful when interpreting the atmospheric absorption. Figure 11 displays the bandpassed-filtered outgoing shortwave flux at TOA. This information is particularly important in understanding the role of the cloud shortwave forcing on the surface energy balance.

Together, all these figures clearly display that on the semiannual timescale, the location of the ITCZ is the main contributor to the variations in the shortwave contribution assuming that the cloud information given in Fig. 9 reflects the convective activities of the ITCZ. It is interesting to note that the shortwave fluxes at the top of the atmosphere and clear air fluxes at the surface are almost out of phase. This is to say that the variations of the clear-sky fluxes are almost entirely dictated by the variation of the cloud shortwave forcing. Atmospheric absorption plays only a minor role in the surface heat balance. This may be the reason why there is a phase difference between the time series of the optical path and that of the clear-sky fluxes. Judging from the variation of the cloudy-sky fluxes at the surface, it is obvious that the surface receives small amount of ra-

diation in the presence of clouds. Most of the solar radiation is reflected back to space as anticipated from the plot of the cloud shortwave forcing.

### *b. 30–60- and 10–25-day oscillations*

The main forcing on the warm pool SST at these timescales is the variation of the solar radiation. The partial percent variance of the solar radiation for this timescale was found to be 67.1% for the 30–60-day and 66% for the 10–25-day oscillations. As done for the semiannual oscillations, cloud content and water vapor path will be used to determine the wet and dry phases of these oscillations. Also shortwave fluxes at TOA in Fig. 11 will be used as an indication of the cloud shortwave forcing.

As opposed to the semiannual timescale, here it is seen that the variation of the optical path is almost out of phase with that of the clear-sky fluxes. In addition to this, strong negative correlation between surface clear-sky fluxes and TOA fluxes is also present at these timescales. The pronounced difference between wet and dry phases in the optical path actually enhances the variations of clear-sky fluxes at the surface through atmospheric absorption. The main reason, however, is the fact that these extreme phases associated with the MJO result in decrease/increase in the cloud cover and thereby the surface fluxes. During the wet phase of the MJO, the incoming solar radiation is mostly absorbed or reflected back to space. Only a small portion of the solar radiation from the clear-sky portion makes its way to the ocean surface. During the dry phase, however, the solar radiation undergoes very little absorption and reflection due to the lower humidity content and mostly clear-sky conditions. As a result, the surface receives much more solar radiation as compared to the wet phase.

Earlier studies (see, e.g., Graham and Barnett 1987; Ramanathan and Collins 1991) have suggested that the cloud shortwave forcing may become large enough in the presence of convective clouds and block the incoming solar radiation. In fact, as mentioned in the introduction, the cloud shortwave forcing is one of the fundamental elements of the thermostat mechanism. These studies often made use of the OLR data as the surrogate for the convection and thereby for the convective clouds. In addition to the OLR data, Ramanathan and Collins (1991) have used observations of the column albedo as cloud shortwave forcing. They were able to show that the solar radiation at TOA is greatly reduced in the presence of highly reflective clouds. Since these types of clouds are strongly related to high SSTs, they further argued that the cloud shortwave forcing acts as a thermostat and inhibits further warming. In relation with this argument, they showed strong correlation between cloud shortwave forcing and SST, especially at high SSTs. Our findings are very similar to the thermostat hypothesis in terms of the role of the cloud shortwave forcing. Note, however, that the cloud longwave forcing has not been mentioned anywhere in this text simply because our initial analysis did not indicate the longwave contribution as an important component. In contrast to the thermostat hypothesis and findings of Tian et al. (2001), our results do not indicate a dipole effect of the cloud radiative forcing. Therefore, our results here and also in the discussion for the semiannual timescale do not confirm the thermostat hypothesis entirely, because this hypothesis also involves uncontrollable warming due to supergreenhouse effect at its initial stage. In contrast, we suggest that the radiative forcing in the surface energy balance be primarily by the solar radiation.

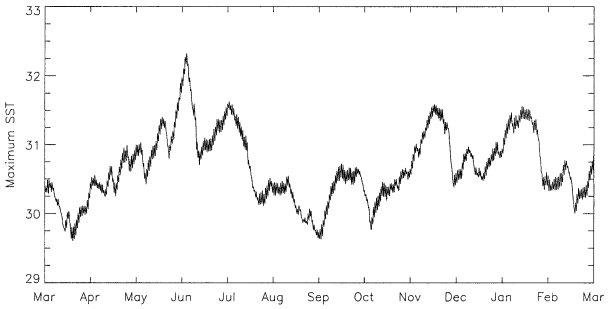


FIG. 12. Time series of the maximum SST over the warm pool region for the same period of the area-averaged SST.

## 8. The regulation of the maximum SST

So far, the important variations in the warm pool SST have been discussed using area-averaged quantities. Recall from the introduction that the most intriguing aspect of the warm pool SST is the capping of the maximum values around 32°C. Therefore, the main topic of this section is to see whether or not we can explain the variations of the maximum SST using those of the area-averaged values. The time variation of the maximum warm pool SST is shown in Fig. 12. This figure clearly illustrates that the types of variations found in the area-averaged warm pool SST also exist in the variation of the maximum SST. All the important variations (semiannual, 30–60, and 10–25 day) can be seen easily. Moreover, the time variation of the maximum SST displays at least three peaks reaching around 32°C during the early summer and winter seasons. As claimed in the observational studies, the maximum SST appears to be capped around 32°C. However, it should be noted that all numerical simulations like ours contain adjustable coefficients that can distort the results dramatically. Therefore, it is hard to prove numerically that the warm pool SST is capped below 32°C. The promising part of our simulation is that it is in very good agreement with the observations over the warm pool area as discussed previously. Such level of accuracy encourages us to construct a regulation mechanism using the findings gathered so far from the FSUCGSM.

On the 10–25- and 30–60-day timescales, the wave

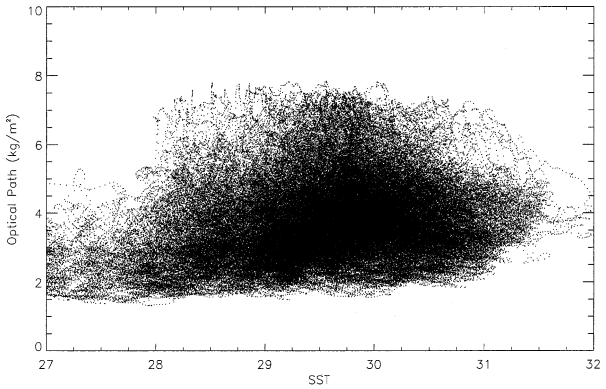


FIG. 13. Scatterplot for optical path of the water vapor vs SST over the warm pool region. The data is a result of FSUCGSM for 1-yr time period sampled every 2 h.

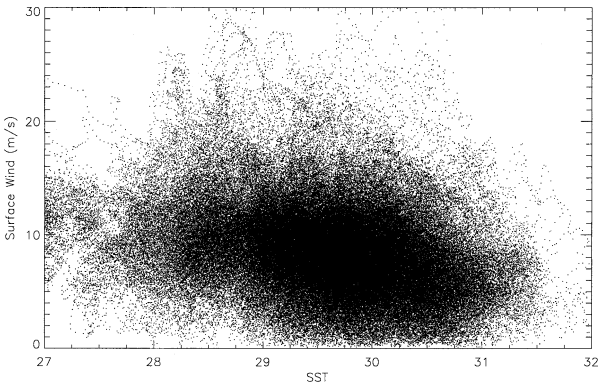


FIG. 14. Same as Fig. 13 except for the surface wind vs SST.

dynamics of the equatorial atmosphere determines the nature of the air–sea interaction and thereby the variations in the SST. The equatorial wave disturbances have widely been studied (Wyrtki 1975; Emanuel 1987; Murakami and Sumathipala 1989; Takayabu 1994; Fasullo and Webster 2000). Even so, the mechanism that triggers these disturbances remains unresolved. Nevertheless, these studies have well established that the 10–25- and 30–60-day oscillations are often associated with easterly traveling waves. Many of these studies have shown that these equatorial waves often alter the atmospheric circulation causing successive westerly and easterly wind anomalies. Moreover, it was shown (Wyrtki 1975; Emanuel 1987; Fasullo and Webster 2000) that the westerly wind anomalies are usually associated with the wet phase of these disturbances and easterly anomalies are associated with the dry phase of the disturbances. Such anomaly wind fields were also noted in our simulation (not shown here).

Considering that the warm pool region is continuously influenced by the wave disturbances, it is inescapable to think that these disturbances constitute the warm pool SST. Ideally, this controlling mechanism works in a way that any increasing tendency of the warm pool SST during the dry (easterly wind anomalies) phase is followed by a decreasing tendency during the wet (westerly wind anomalies) phase. The compensation between two successive phases is often disturbed by other processes such as wave–wave interaction. Therefore, the net variations on each timescale may display a rather wide range of magnitudes.

Unlike the wave disturbances discussed above, the semiannual timescale is dictated heavily by the convective processes associated with the ITCZ. As seen in Fig. 6, the largest variations of the warm pool SST occur in this timescale. This variation is much more recurrent than those of the 10–25- and 30–60-day timescales probably because the main cause is rooted in the annual variations of the incoming solar radiation. Unless there is a sizable change in the incoming solar radiation, the variations of the warm pool SST at the semiannual timescale are strictly controlled.

In summary, the 10–25-, 30–60-day, and semiannual oscillations may impose certain restrictions on the maximum SST over the warm pool. One of the clear evidences for this is their continuous influences of these variations over this region. This may be a necessary condition for capping the maximum SST but not sufficient enough to complete the discussion. The magnitudes of these oscillations should also be bounded such a way that they will not cause the SST to shoot over the maximum limit. One way we can check the magnitude is to plot the scatter diagrams of the SST versus the most influential variables (i.e., atmospheric moisture, surface wind, and moisture deficit). These plots will provide sufficient information on the variation of these important elements when the SST gets closer to its upper limit. The diagrams are displayed in Figs. 13–15.

First, from the scatterplot of SST versus the optical path of the water vapor, it is possible to identify three distinct regimes. The first regime is when the SST is between 27° and 28°C, where the atmospheric moisture content is at its lowest level. This is followed by the convective regime where SST is between 28° and 29.5°C. In this region, atmospheric moisture content in-

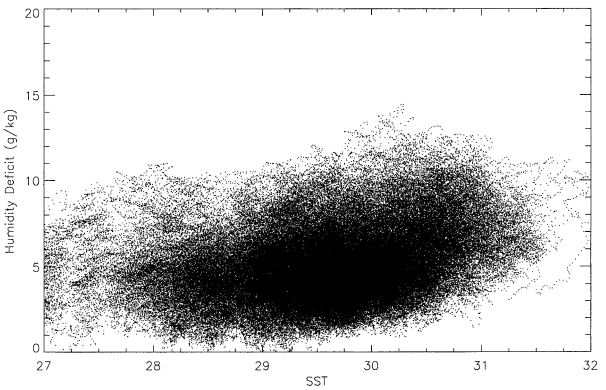


FIG. 15. Same as Fig. 13 except for the moisture deficit vs SST.

creases substantially with increasing temperature. Beyond 29.5° is the third regime where the moisture content displays a decreasing trend. These regimes are remarkably similar to those found observationally (Graham and Barnett 1987; Waliser and Graham 1993; Waliser 1996; Lau et al. 1997) as discussed in the introduction. Second, for Figs. 13–15 the great portion of the scatterplots lies roughly between 28° and 31°C and the contributions hardly lead SST beyond these values. Furthermore, all these figures clearly display that the variations beyond these threshold temperature values are very small as compared to the variations in the convective regime. This can be depicted judging from the spread of the scatterplots at high and low SSTs.

All these results point to the important conclusion that the tendencies that drive the warm pool SST have their most active state, and thereby the largest variations, when the SST is roughly in the range of 28°–31°C. Beyond this range the contributions, and thereby the SST, have very low variability. Judging from the scatterplots, it might also be argued that the warm pool SST mostly stays between 28° and 31°C. Thus, it is probably more appropriate to describe the first and third regions as transition zones rather than as 2 of 3 regimes of the warm pool SST. In the nonconvective region, where the SSTs are around the minimum values, the sea surface receives maximum amount of radiation. Although the surface winds are high, the evaporative cooling is negligible because of the low moisture deficit due to the cold temperatures. Therefore, solar heating causes the SST to increase. Consequently, convective measures such as increasing moisture content of the atmosphere, developing low-level convergence (decreasing winds), and increasing moisture deficit become prominent when the SST reaches around 29°C. In the temperature range of 29°–30°C, these convective measures clearly define the convective activities. All these features can be seen in the time series of the direct and indirect contributions shown earlier. The SST range of 30°–32°C is characterized by the diminishing convective measures. The role of the evaporative cooling and solar heating at this stage of the convective phase is to cool the SST. Thus, SSTs between 30° and 32°C are the highest values that can ever be reached. Despite the cooling of the SST, convection may continue until the SSTs decrease to a point where the atmosphere cannot sustain upward motion and all available potential moisture in the atmosphere is consumed by demoisturization processes. SSTs approximately from 29° to 32°C and then from 32° to 29°C, respectively, coincide with the intensification and weakening stages of the convective systems. Also, maximum SSTs tend to occur during the transition from intensification to weakening stages. After the passage of the convective systems, the conditions for the dry phase begin to emerge. The initial stage of the dry phase involves further cooling due to very large evaporative fluxes. As SSTs become cooler the evaporative cooling becomes smaller. Lack of convective clouds lets the surface of the ocean receive solar radiation that eventually causes the SST to increase. Thus, similar to the convective phase, the nonconvective phase coincides with SSTs approximately from 29° to 27°C and then, from 27° to 29°C, respectively, the initial and final stages of the dry phase.

The interpretation given above explains the main mechanism of how warm pool SST oscillates between its maximum and minimum values. It should be noted that the maximum and minimum for each cycle of the modes may differ slightly. For example, during early summer, when SSTs are close to the upper limit, the 10–25- or 30–60-day oscillations will probably let the SSTs oscillate between 32° and 29°C. In this case, SSTs are concentrated between 29° and 32°C. Conversely, during early winter, SSTs are very close to the lower limit and are concentrated between 27° and 29°C. Apart from these extreme cases, SSTs generally stay between 28° and 31°C as can also be perceived from the dark areas of Figs. 13–15.

In summary, the results from our numerical simulation suggest that the warm pool SST oscillates between certain threshold values. As implied by these variations, it is highly possible that there is an upper limit to the warm pool SST. Furthermore, our results also suggest a lower limit around 27°C that can be anticipated from Figs. 13 to 15. The main process that maintains this balance is the convection associated with these important timescales described before. These oscillations seem to be continuously reproduced in time. The continuity of the semiannual variations is straightforward since it is related to the annual variation of the solar radiation. In the presence of the equatorial waveguide the intraseasonal variations are also expected to be continuous in time. Such conditions are well represented by our simulation.

## 9. Summary and conclusions

The FSUCGSM is utilized to study the possible regulation of the maximum SST over the warm pool. For this goal, we first identified all terms that contribute to the warm pool SST. This procedure is done in a way that the SST balance equation becomes residue free. The results of a 1-yr time integration of the FSUCGSM are used to obtain the time evolutions of the residue-free warm pool SST and its contributors. To ensure the validity of the coupled model, the NCEP SST analysis for the period of the model integration is compared with the model-predicted SST. Overall the comparison displayed good agreement with the NCEP analysis. The best agreement was seen over the western equatorial Pacific. Such good agreement has demonstrated that the FSUCGSM is able to capture most of the dynamical and physical processes over the equatorial Pacific on an annual timescale.

It was found that the warm pool SST is derived mainly by three important types of oscillations, namely, semi-

annual, 30–60-, and 10–25-day oscillations. Then, the results of combined Butterworth bandpass filter and EOF analysis have revealed that the tendency of the solar radiation is the primary cause of the high-frequency oscillations (10–25 and 30–60 day) and the secondary cause for the low-frequency oscillations (semiannual). Moreover, the evaporative cooling was found to be the primary cause of the low-frequency oscillations and secondary cause of the high-frequency oscillations. Thus, it was concluded that the possible regulation mechanism of the warm pool SST can be explained by examining only the tendencies of the solar radiation and evaporative cooling.

The variations of the cloud cover in relation with the atmospheric moisture content, surface wind, and humidity deficit were found to be the most important factors relating the changes in the SST to those in the convective activities. In relation with the atmospheric moisture content, it was found that the cloud shortwave forcing plays the most crucial role on the solar radiation at the surface.

In the light of these findings, it is proposed that the warm pool SST may have an upper limit as suggested by previous authors. In addition, our findings indicated that there may also be a lower limit at around 27°C.

To our knowledge, our study is the most detailed numerical study ever done concerning the regulation of the warm pool SST. We have benefited from both observational findings and model simulation. Unlike the previous studies, we have used coupled global atmosphere–ocean models and analyzed each contribution individually. As stated by earlier authors, one of the advantages of using coupled GCMs is that the comparison among the terms in the SST equation can be done efficiently without worrying about datasets being from different sources. Also, all diagnostic and prognostic variables that are indirectly related to the SST can be analyzed instantly. However, there is more to be done. For instance, the resolution we have used in our study does not permit the narrow-canal coastal currents that seem to be very important in simulating the ocean circulation. Also, the cloud parameterization scheme used in this model does not adequately consider mesoscale convective processes abundant over the warm pool region. Thus a similar study with higher resolution and a better cumulus parameterization scheme might be the next step toward understanding the real nature of the warm pool SST.

*Acknowledgments.* This research was supported by NASA Grant NAG1-2127, NSF Grant ATM-9612894, NOAA Grant NA86GPO031, and NOAA Grant NA96GPO400. Special thanks go to Dr. H. S. Bedi of FSU for his endless support on the FSU Global Spectral Model and Dr. T. LaRow of FSU for his support on the MPI ocean model. Also, we thank NCAR Scientific Data Division for providing the NCEP and ECMWF analyses.

## REFERENCES

Arakawa, A., and V. R. Lamb, 1977: Computational design of the basic dynamical processes of UCLA General Circulation Model. *J. Comput. Phys.*, **16,** 173–263.

Arking, A., and D. Ziskin, 1994: Relationship between clouds and sea surface temperatures in the western tropical Pacific. *J. Climate,* **7,** 988–1000.

Businger, J. A., J. C. Wyngaard, Y. Izumi, and E. F. Bradley, 1971: Flux–profile relationship in the atmospheric surface layer. *J. Atmos. Sci.,* **28,** 181–189.

Cubukcu, N., 2001: Low frequency controls on the thresholds of sea surface temperature over the western tropical Pacific. Ph.D. dissertation, The Florida State University, 136 pp. [Available from Dirac Science Library, The Florida State University, Tallahassee, FL 32306.]

Emanuel, K. A., 1987: An air–sea interaction model of intraseasonal oscillations in the Tropics. *J. Atmos. Sci.,* **44,** 2324–2340.

Fasullo, J., and P. J. Webster, 2000: Atmospheric and surface variations during westerly wind burst in the tropical western Pacific. *Quart. J. Roy. Meteor. Soc.,* **126,** 899–924.

Gadgil, S., P. V. Joseph, and N. V. Joshi, 1984: Ocean–atmosphere coupling over the monsoon regions. *Nature,* **358,** 394–397.

Graham, N. E., and T. P. Barnett, 1987: Sea surface temperature, surface wind divergence and convection over tropical oceans. *Science,* **238,** 657–659.

Harshvardhan, and T. G. Corsetti, 1984: Long wave parameterization for the UCLA/GLAS GCM. NASA Tech. Memo. 86072, Goddard Space Flight Center, 51 pp. [Available from NASA Goddard Space Flight Center, Greenbelt, MD 20771.]

Hartmann, D. L., and M. L. Michelsen, 1993: Large-scale effects on the regulation of tropical sea surface temperature. *J. Climate,* **6,** 2049–2062.

Knox, R. A., and D. Halpern, 1982: Long-range Kelvin wave propagation of transport variations in the Pacific Ocean equatorial currents. *J. Mar. Res.,* **40,** 329–339.

Krishnamurti, T. N., and D. Subrahmanyam, 1982: The 30–60 day mode at 850 mb during MONEX. *J. Atmos. Sci.,* **39,** 2088–2095.

——, and S. Gadgil, 1985: On the structure of the 30–50 day mode over the globe during FGGE. *Tellus,* **37A,** 336–360.

——, S. Low-Nam, and R. Pash, 1983: Cumulus parameterization and rainfall rates II. *Mon. Wea. Rev.,* **111,** 815–828.

——, H. S. Bedi, and D. V. M. Hardiker, 1998: *An Introduction to Global Spectral Modeling.* Oxford University Press, 253 pp.

——, D. Bachiochi, T. E. LaRow, B. Jha, M. Tewari, D. R. Chakraborty, R. Correa-Torres, and D. Oosterhof, 2000: Coupled atmosphere–ocean modeling of the El Niño of 1997–98. *J. Climate,* **13,** 2428–2459.

Krueger, A. F., and T. I. Gray Jr., 1969: Long-term variations in equatorial circulation and rainfall. *Mon. Wea. Rev.,* **97,** 700–711.

Lacis, A. A., and J. E. Hansen, 1974: A parameterization for the absorption of solar radiation in the earth's atmosphere. *J. Atmos. Sci.,* **31,** 118–133.

LaRow, T. E., and T. N. Krishnamurti, 1998: Initial conditions and ENSO prediction using a coupled ocean–atmosphere model. *Tellus,* **50A,** 76–94.

Latif, M., T. Stockdale, J. Wolff, G. Burgers, E. Maier-Reimer, M. Junge, K. Arpe, and L. Bengtsson, 1994: Climatology and variability in the ECHO coupled GCM. *Tellus,* **46A,** 351–366.

Lau, K.-M., and C.-H. Sui, 1997: Mechanisms of short-term sea surface temperature regulation: Observations during TOGA COARE. *J. Climate,* **10,** 465–472.

——, ——, and W.-K. Tao, 1994: An inquiry into the cirrus-cloud thermostat effect for tropical sea surface temperature. *Geophys. Res. Lett.,* **21,** 1157–1160.

——, H.-T. Wu, and S. Bony, 1997: The role of large-scale atmospheric circulation in the relationship between tropical convection and sea surface temperature. *J. Climate,* **10,** 381–392.

Levitus, S., 1982: *Climatological Atlas of the World Ocean.* NOAA Prof. Paper 13, 173 pp. and 17 microfiche.

Madden, R. A., and P. R. Julian, 1971: Description of a 40–50 day oscillation in the zonal wind in the tropical Pacific. *J. Atmos. Sci.,* **28,** 702–708.

——, and ——, 1972: Description of global-scale circulation cells in the tropics with a 40–50 day period. *J. Atmos. Sci.,* **29,** 1109–1123.

McPhaden, M. J., and B. A. Taft, 1988: Dynamics of seasonal and intraseasonal variability in the eastern equatorial Pacific. *J. Phys. Oceanogr.,* **18,** 1713–1732.

Murakami, M., 1979: Large-scale aspects of deep convective activity over the GATE area. *Mon. Wea. Rev.,* **107,** 994–1013.

Murakami, T., and W. L. Sumathipala, 1989: Westerly bursts during the 1982/83 ENSO. *J. Climate,* **2,** 71–85.

Newell, R. E., J. W. Kidson, D. G. Vincent, and G. J. Boer, 1972: *The General Circulation of the Tropical Atmosphere and Interaction with Extratropical Latitudes.* Vol. 1. Massachusetts Institute of Technology, 258 pp.

Ramanathan, V., and W. Collins, 1991: Thermodynamic regulation of ocean warming by cirrus clouds deduced from observations of the 1987 El Nino. *Nature,* **351,** 27–32.

Schneider, N., T. Barnett, M. Latif, and T. Stockdale, 1996: Warm pool physics in a coupled GCM. *J. Climate,* **9,** 219–239.

Sterl, A., 1991: Manual for the primitive equation OGCM as used for ENSO studies and the interface of ECHAM. Max-Planck-Institut für Meteorologie, Hamburg, Germany, 58 pp.

Sud, Y. C., G. K. Walker, and K.-M. Lau, 1999: Mechanisms regulating sea-surface temperatures and deep convection in the Tropics. *Geophys. Res. Lett.,* **26,** 1019–1022.

Takayabu, Y. N., 1994: Large-scale cloud disturbances associated with the equatorial waves. Part I: Spectral features of the cloud disturbances. *J. Meteor. Soc. Japan,* **72,** 433–448.

Tian, B., G. J., Zhang, and V. Ramanathan, 2001: Heat balance in the Pacific warm pool atmosphere during TOGA COARE and CEPEX. *J. Climate,* **14,** 1881–1893.

Tiedtke, M., 1984: The sensitivity of the time-mean large-scale flow to cumulus convection in the ECMWF model. *Proc. Workshop on Convection in Large-Scale Numerical Models,* Reading, United Kingdom, ECMWF, 297–316.

Waliser, D. E., 1996: Formation and limiting mechanisms for very high sea surface temperatures: Linking the dynamics and thermodynamics. *J. Climate,* **9,** 161–188.

——, and C. Gautier, 1993: A satellite-derived climatology of ITCZ. *J. Climate,* **6,** 2162–2174.

——, and N. E. Graham, 1993: Convective cloud systems and warm-pool sea surface temperatures: Coupled interaction and self-regulation. *J. Geophys. Res.,* **98,** 12 881–12 893.

Wallace, J. M., 1992: Effect of deep convection on the regulation of tropical sea surface temperature. *Nature,* **357,** 230–232.

Wyrtki, K., 1975: El Niño—The dynamical response of the equatorial Pacific Ocean to atmospheric forcing. *J. Phys. Oceanogr.,* **5,** 572–584.

Zangvil, A., 1975: Upper tropospheric waves in the Tropics and their association with clouds in the wavenumber–frequency domain. Ph.D. thesis, University of California, Los Angeles, 131 pp.

Zhang, G. J., and M. J. McPhaden, 1995: The relationship between sea surface temperature and latent heat flux in the equatorial Pacific. *J. Climate,* **8,** 589–605.

——, V. Ramanathan, and M. J. McPhaden, 1995: Convection–evaporation feedback in the equatorial Pacific. *J. Climate,* **8,** 3040–3051.